Research Square

Preprints are preliminary reports that have not undergone peer review.
They should not be considered conclusive, used to inform clinical practice,
or referenced by the media as validated information.

# A Theoretical Investigation of Excited State Kinematics and Optoelectronic Properties of Gold-Centered Carbene Metal Amides for Thermally Activated Delayed Fluorescence

**Kazi Mahmudur Rahman**
Shahjalal university of Science and Technology
**Muhammed Sakil Hussain**
Shahjalal university of Science and Technology
**Nazia Chawdhury**
nc-phy@sust.edu

Shahjalal university of Science and Technology

**Research Article**

**Keywords:** Reverse Intersystem Crossing, Thermally Activated Delayed Fluorescence, Density Functional Theory, Organic Light Emitting Diodes

**Posted Date:** August 18th, 2026

**DOI:** https://doi.org/10.21203/rs.3.rs-10460431/v1

**License:** This work is licensed under a Creative Commons Attribution 4.0 International License.
Read Full License

**Additional Declarations:**
No competing interests reported.

Tables 1 is available in the supplementary files section

# A Theoretical Investigation of Excited State Kinematics and Optoelectronic Properties of Gold-Centered Carbene Metal Amides for Thermally Activated Delayed Fluorescence

Kazi Mahmudur Rahman[1], Muhammed Sakil Hussain[1], Nazia Chawdhury[1]

*[1]Department of Physics, Shahjalal university of Science and Technology, Sylhet-3114, Bangladesh*

Corresponding Author: Nazia Chawdhury
Email: nc-phy@sust.edu

## Abstract

**Context:** In recent years, studies have been conducted to explore the mechanism of Thermally Activated Delayed Fluorescence to develop efficient organic light emitting diodes. This research aims to systematically explore the role of spin-orbit coupling in electronic, optical, and kinetic properties of five gold-centered carbene metal amides of varying carbazole ligands while also evaluating their potential of turning out to be effective Thermally Activated Delayed Fluorescence emitters. In this study, the highest rate of reverse intersystem crossing $10^8$ $s^{-1}$ has been obtained for the most fundamental molecule of gold-centered carbene metal amide (CMA1), making it a perfect candidate to be a TADF emitter. However, its low absorption and emission intensity is a concern. By adding side chains to the donor ligands, we have achieved higher emission intensity at the cost of lower rate of reverse intersystem crossing, and reached suitable property for perfect lighting device applications.

**Method:** Utilizing DFT in Gaussian 16w software, we optimized the molecular structure and found the computational electronic structure, absorption spectra, and fluorescence spectra. In these simulations, we used APFD functional and mixed basis sets - SVP for C, H and O, while SDD for Au atom. Using B3LYP functional and mixed basis sets (DEF-2 TZVP for H, C, O and N, while ZORA-TZVP for Au) in ORCA 5 software, we found the computational electronic structure including triplet state splitting via spin-orbit coupling and also attained the spin-orbit coupling matrix element values. The rates of reverse intersystem crossing were calculated using Marcus-Levich equation.

**Keywords:** Reverse Intersystem Crossing, Thermally Activated Delayed Fluorescence, Density Functional Theory, Organic Light Emitting Diodes

## Introduction

As researchers all over the world are trying to move towards more environmentally friendly solutions and practices, organic optoelectronic devices are becoming increasingly demanding day by day. For a new generation of technology, organic light-emitting diodes (OLEDs) are very promising candidates for smart display applications and energy-saving light sources in the coming years [1-2]. Therefore, many organic molecules that manifest optical properties, such as fluorescence and phosphorescence, have been explored in the last few decades [3-5]. Scientists are actively looking for ways to maximize fluorescence. Theoretically, spin statistics show that electrical excitations result in the formation of ~25% singlet excitons and ~75% triplet excitons. Spin allowed radiative transition of the singlet excitons to the ground state showing only fluorescence, which led to the discovery of first-generation OLEDs in 1990 [6, 7]. Therefore, to achieve higher electroluminescence from OLEDs, one is required to convert spin-forbidden transitions to spin-allowed by incorporating heavy metal atoms in the organic complexes. This enhances spin-orbit coupling (SOC), which leads to intersystem crossing (ISC) from the singlet excited state to the triplet excited state [ 8, 9].

Perrin first observed thermally activated delayed fluorescence (TADF) in 1929 [10] in fluorescein solution and uranyl salts. TADF materials can have immensely enhanced fluorescence due to their unique property of utilizing both singlet and triplet excitons. In such molecules, triplet excitons are thermally converted into singlet excitons through a process called reverse intersystem crossing (rISC) by exploiting a very small singlet-triplet energy gap ($\Delta E_{st}$) and large separation between the Highest Occupied Molecular Orbital (HOMO) and the Lowest Unoccupied Molecular Orbital (LUMO) [11]. Since the beginning of the twenty-first century, tremendous efforts have been made to develop TADF emitters and incorporate them into third-generation

OLEDs [12-14]. A theoretical study in 2021 revealed that effective rISC takes place when $\Delta E_{st}$ is approximately equal to reorganization energy (λ) [15]. Additionally, SOC plays a crucial role in determining the rate of reverse intersystem crossing ($K_{rISC}$) [16-18]. Molecules having extremely high values of $K_{rISC}$ are considered to be effective TADF materials. The figure 1 below illustrates the mechanism of TADF.

In the last few decades, carbazole derivatives became quite popular in the field of organic optoelectronics due to their properties which allow for high structural modification and large HOMO-LUMO separation [19-20]. This led to numerous studies of carbene metal amides (CMAs) as potential TADF materials for applications in optoelectronics. CMAs consist of carbene and amide ligands which are linked by a heavy metal atom. Linear geometry of heavy metal complexes enables rotational flexibility, which allows tunability of the energy gap between singlet and triplet excited states [21]. In such molecules, carbene acts as an electron acceptor whereas the amide acts as electron donor [22]. Heavy metals are known to enhance the SOC, leading to more efficient rISC [23]. Föller et al., calculated intersystem and reverse intersystem crossing rates in gold-centered cyclic alkyl amino carbene carbazole complex in solid state and in various solvents, and found efficient fluorescence emission without internal ligand rotation in solid states [24]. Taffet et al., computationally studied the singlet and triplet geometries of copper-centered CMAs to understand their impact on singlet-triplet gap and spin-orbit coupling [25]. Li et al., carried out a structural investigation of carbene metal amides to see how the presence of nitrogen atoms affects TADF properties in them [26]. Zobel et al., calculated $\Delta E_{st}$ values to investigate TADF mechanism in some Cu centered CMAs [27]. They studied torsional motion rigorously in both singlet and triplet geometries. Photoluminescence efficiencies >99% and microsecond lifetimes were achieved for Cu(I) centered CMA in which carbazole was used as donor ligand [28]. Previously, computational studies reported a $K_{rISC}$ value of $8.81 \times 10^6$ $s^{-1}$ and $1.74 \times 10^9$ $s^{-1}$ for Cu centered CMA at 298K [29-30]. Therefore, CMAs are very promising for applications in high-efficiency third-generation OLEDs.

In this work, we took five different gold-centered carbene metal amides (CMAs) and studied their optoelectronic properties to determine their potential as effective TADF materials. The molecules are composed of cyclic (alkyl)(amino)carbene (CAAC) and four derivatives of various carbazole ligands with gold atoms as the bridge between them. Previous studies revealed that the gold center plays a significant role in stabilizing the excited states and its unique electronic configuration leads to strong spin-orbit coupling which enhances rISC and promotes efficient TADF [31-32]. However, there is a lack of systematic study of how singlet-triplet energy gap and spin-orbit coupling affect rISC in gold CMAs. According to Kasha's rule, photon emission, like fluorescence and phosphorescence, takes place from the lowest excited states. In 1950, it was found that internal conversion is about ten thousand times faster than spontaneous emission from higher excited singlet states, and it is claimed that the reverse intersystem crossing generally takes place from $T_1$ to $S_1$ state [33]. However, SOC can heavily influence the rate of reverse intersystem crossing. As a result, it is possible that strong SOC can lead to faster rISC between higher excited singlet-triplet states. There are several reports of rISC from higher excited triplet states [34-35]. In cases where the $T_1$-$T_2$ energy gap is larger than that between $S_2$ and $T_2$, rISC from $T_2$ to $S_2$ becomes more probable, followed by internal conversion (IC) from $S_2$ to $S_1$ [36]. Energy gap law [37] suggests that the IC from higher lying triplet excited states to the first triplet excited state, such as $T_2 \rightarrow T_1$ is usually very fast ($\sim 10^{12}$ $s^{-1}$) when the $T_2$-$T_1$ energy gaps of CMAs are small i.e., less than 1 eV. Therefore, in this study, we have calculated $K_{rISC}$ from the lowest triplet excited state to the first singlet excited state, as small energy gaps have been observed between $T_1$ and higher triplet states.

## Methodology

Our work uses a computational approach using Gaussian 16w and ORCA 5 simulation software packages to explore the potential of gold-centered CMAs as TADF emitters. We used DFT to optimize the geometries of the molecules at the ground state and time-dependent DFT to calculate the excited singlet and triplet state energies of the molecules at ground state geometry, as well as to optimize the geometry at excited $S_1$ and $T_1$ states. The energy difference between the optimized $T_1$ and $S_1$ states gives the $\Delta E_{st}$ value. To perform these calculations, we utilized the Austin-Frisch-Petersson functional with dispersion corrections (APFD) functional and mixed basis sets, SVP basis set was used for C, H and O, while SDD basis set was used for Au, in Gaussview6 and Gaussian 16w [38] software. APFD is a hybrid functional that includes dispersion corrections, increasing its accuracy in modelling non-covalent interactions like Van der Waals forces. It avoids excessive long-range attractive or repulsive interactions, unlike other dispersion-corrected functionals, leading to more realistic geometries [39]. Thus, this increases accuracy in molecules like CMAs in which metal-ligand interactions play a crucial role. Moreover, APFD being computationally less expensive, can provide results faster while maintaining reasonable reliability, making it suitable for my large molecules. Additionally, an effective core potential (ECP) was used for Au. To optimize the geometry of these molecules at triplet states, we used unrestricted spin in the GaussView6 calculation setup. No solvents were used in these simulations. From these calculations, we also extracted HOMO-LUMO energy gaps, optical absorption spectra and fluorescence emission spectra for each molecule.

We obtained SOCME and spin-orbit interaction energy values using ORCA 5 software [40] utilizing Becke, 3-parameter Lee-Yang-Parr (B3LYP) functional and mixed basis sets. DEF-2 TZVP basis set was used for H, C, O and N while ZORA-TZVP basis set was used for Au. Zero-order relativistic approximation (ZORA) and Segmented All-electron Relativistic Core (SARC) were implemented to account for relativistic effects in calculations and achieve higher accuracy. Moreover, we obtained spin orbit coupling corrected optical absorption spectra from these calculations.

The values of $K_{rISC}$ can be calculated using the following equation:

$$K_{rISC} = \frac{2\pi}{\hbar} \mid \xi_{st} \mid^2 \cdot \frac{1}{\sqrt{4\pi\lambda_{rISC}k_BT}} \cdot \sum_{n=0}^{\infty} e^{-S}\frac{S^n}{n!} \cdot exp\left[-\frac{(\Delta E_{st}+\lambda_{rISC}+n\hbar\omega_{eff})^2}{4\lambda_{rISC}k_BT}\right] \quad (1)$$

where $\lambda_{rISC}$ is the reorganization energy for rISC process, $k_B$ is the Boltzmann constant, $\hbar$ is the reduced Planck's constant, T is the temperature in Kelvin, $\hbar\omega_{eff}$ is the effective energy of a mode representing the relevant nonclassical high-frequency intramolecular vibrations and S is the effective Huang-Rhys factor and n is an integer (n=0,1,2…).

The Franck-Condon factor $e^{-S}\frac{S^n}{n!} = \mid < \omega_{vib,f} \mid \omega_{vib,i} > \mid^2$ gives the probability of the transition from the 0th vibrational level of the ground state to the nth vibrational level of the excited state.

$\xi_{st}$ is the SOCME value between $S_1$ and $T_1$. For the case of strong spin-orbit coupling, we can use the Marcus-Levich equation [15]:

$$K_{rISC} = \frac{1}{\hbar} \mid \xi_{st} \mid^2 \cdot \sqrt{\frac{\pi}{\lambda_{rISC}\,K_BT}} \cdot exp\left[-\frac{(\Delta E_{st}+\lambda_{rISC})^2}{4\lambda_{rISC}\,K_B\,T}\right] \quad (2)$$

A recent report showed the activation energy (△G) is a much better parameter for determining the potential of a molecule to be a good TADF material [15]. Activation energy is expressed as:

$$\triangle G = \frac{(\Delta E_{st}+\lambda_{rISC})^2}{4\lambda_{rISC}} \quad (3)$$

The reorganization energy for rISC from $T_1$ to $S_1$ was calculated using Gaussian 16w. First, we optimized the geometry of the molecules in the $T_1$ and $S_1$ states using TD-DFT and then calculated the energy of the $S_1$ state at the $T_1$ optimized geometry as shown in Figure 2. The following equation is used to calculate the reorganization energy $\lambda_{rISC}$.

$$\lambda_{rISC} = E_{T1}^{S1} - E_{S1}^{S1} \quad (4)$$

where $E_{T1}^{S1}$ is the energy of the $S_1$ state of the molecule at the optimized $T_1$ geometry and $E_{S1}^{S1}$ is the energy of $S_1$ state at $S_1$ optimized geometry.

## Results and Discussion

The molecular and optimized structures are shown in Figure 3 of the investigated donor-acceptor type CMAs where cyclic (alkyl) (amino) carbene (CAAC) ligand acts as acceptor and the carbazole ligands as donor. Here, we consider CMA1 as the mother gold-centered carbene metal amide without any additional functional groups in the carbazole ligands. We have designed the molecules with different functional groups in the ligands aiming to obtain enhanced TADF emission. Figure 4 confirms the donor-acceptor character of the molecules. Here, HOMO and LUMO are well separated at the ground state geometry with the highest energy separation of 3.47 eV for CMA5 and that of lowest for CMA2. We observe that CMA1 and CMA2 show much better donor-acceptor properties. However, the LUMOs of CMA3, CMA4 and CMA5 are not perfectly centered on acceptor units.

The energy level diagram of the first five lower lying excited singlet and triplet states at ground state geometry is shown in Figure 5. Smaller energy gap between the first excited triplet and first excited singlet state is crucial for effective rISC [11].

We observe that CMA1, CMA2, CMA3 have energy gaps between $S_1$ and $T_1$ within 0.3 eV while CMA4 and CMA5 have larger gaps of about 0.4 eV. We find for our molecules that there is a relation between the donor-acceptor character and the energetic position of excited triplet states relative to first excited singlet state. Comparing Figure 5 with Figure 4, we see that the CMA1 and CMA2, both of which have good donor-acceptor properties, show one triplet state below $S_1$, whereas other molecules have multiple excited triplet states below $S_1$.

Heavy metal atoms, due to their high nuclear charge, lead to stronger spin-orbit coupling which increases the splitting of the triplet sublevels due to the interaction of spin angular momentum and orbital angular momentum as shown Figure 6. The spin-orbit interaction energy is given by the Hamiltonian:

$$H_{soc} = \xi(\overrightarrow{r})\,(\vec{l}\cdot\vec{s}\,) \quad (5)$$

where $\vec{l}$ is the orbital angular momentum, $\vec{s}$ is the spin angular momentum and $\xi(\overrightarrow{r})$ is the spin-orbit coupling constant.

Figure 6 illustrates that $T_1$ sublevels of CMA1 exbibit the largest splitting compared to other molecules which could arise from the relatively stronger SOC between $T_1$ and $S_1$ states as shown in Table 1. The SOC induces mixing of the excited singlet and triplet states, which can alter their energies [41] as evidenced here by the differences observed between the calculated energy values obtained with and without consideration of it. Moreover, this behavior can significantly influence the rates of rISC by modifying the $\Delta E_{st}$ values alongside the direct effect of SOC strength according to equation 2.

The shift in energy of $S_1$ and $T_1$ states due to SOC is approximately given by the following equations:

$$\Delta E(S_1) \sim \frac{|\langle T_n \rangle|^2}{E_{S_1} - E_{T_n}} \quad (6)$$

$$\Delta E(T_1) \sim \frac{|\langle S_n \rangle|^2}{E_{T_1} - E_{S_n}} \quad (7)$$

Where $|\langle T_n \rangle|$ is the spin-orbit coupling matrix element (SOCME) between the singlet excited state $S_1$ and nth triplet excited state $T_n$, $|\langle S_n \rangle|$ is the SOCME between the triplet excited state $T_1$ and nth singlet excited state $S_n$, $E_{T_n}$ is the energy of nth excited triplet state and $E_{S_n}$ is the energy of the nth excited singlet state.

According to equations (6) and (7), a stronger SOC and a smaller singlet-triplet energy gap produces a larger SOC-induced energy shift. The sign of the denominator determines whether the perturbed energy increases or decreases. For example, in the case of $S_1$ state, a positive denominator ($E_{S1}$-$E_{Tn}$ > 0) results in an increase in the $S_1$ energy, whereas a negative denominator ($E_{S1}$-$E_{Tn}$ < 0) leads to a decrease in the $S_1$ energy.

We observe that the $S_1$ energy decreases slightly for CMA1, CMA2, and CMA3 when SOC is included as the gap between $S_1$ and lower-lying triplet states is much smaller than that between $S_1$ and the higher triplet states. As a result, $S_1$ interacts predominantly with these lower triplets, forming admixtures and being stabilized through SOC-induced mixing. In contrast, for CMA4 and CMA5, the $S_1$ energy shows a slight increase upon inclusion of SOC since they have relatively small energy separations between $S_1$ and a higher excited triplet state ($T_3$) leading to a small upward shift in the perturbed energy. For all molecules, the $T_1$ energy decreases when SOC is taken into account which is consistent with the perturbation expression, where $T_1$ interacts mainly with $S_1$ that lie above it, causing a downward stabilization.

Theoretical absorption and photoluminescence (PL) spectra for fluorescence emission of the CMAs are presented in Figure 7. The optical absorption peaks are at 2.56 eV, 2.40 eV, 2.70 eV, 2.59 eV and 2.57 eV for CMA1, CMA2, CMA3, CMA4 and CMA5 respectively, and the oscillator strengths for transition from $S_0$ to $S_1$ are 0.14, 0.19, 0.29. 0.30, and 0.22 for these molecules respectively. The corresponding emission peaks are in the visible region, especially CMA3, CMA 4 and CMA 5 show a broad spectrum emitting white light. This is due to the chemical modification by introducing side chains in fundamental CMA1. Meanwhile, CMA1 and CMA2 show narrow emission bands. We also find that the intensity of the emission spectra can be increased significantly and tuned by varying the carbazole ligand. However, this also reduce the rate of rISC in the modified structures as can be seen in Table 1. Therefore, it is crucial to maintain a balance between $K_{rISC}$ value and PL intensity introducing challenges in materials design. Analyzing Figure 7 and Table 1, we find that CMA3

shows the highest emission intensity and the highest value of $K_{rISC}$ among the modified structures making it most suitable for light-emitting device applications.

Figure 8 shows the HOMO and LUMO of each molecule at optimized $S_1$ and $T_1$ geometry. A large HOMO-LUMO separation ($\Delta E_{HL}$) is observed in the optimized excited state geometries, which facilitates the rISC process. The modified structures exhibit wider HOMO-LUMO energy separation at excited state geometries compared to the HOMO-LUMO separation of CMA1. In each molecule, the HOMO energy ($E_H$) is observed lower at $T_1$ geometry compared to $S_1$ geometry, as expected. While CMA1, CMA2 and CMA5 show good spatial separation between HOMO and LUMO, CMA3 and CMA4 show some partial spatial overlap between HOMO and LUMO.

Figure 9 shows that at 298.15K, the value of $K_{rISC}$ decreases as the activation energy increases. The relationship between activation energy and $K_{rISC}$ is almost linear with a negative slope. This is consistent with the theory because as activation energy increases, more energy is required for reverse intersystem crossing to occur, hence the rate of rISC decreases. CMA3 and CMA4 have similar activation energy values, however, the larger SOCME value of CMA3 results in a higher $K_{rISC}$ value. This clearly demonstrates that stronger SOC leads to more effective rISC. There is no data for CMA5 since neither activation energy nor $K_{rISC}$ could be calculated for this molecule as we could not optimize it at $T_1$ state using time-dependent self-consistent field method in gaussian 16w due to fact that the calculation was not converging.

Analyzing Table-1, we see that the gold atom enhances spin-orbit coupling in CMAs. CMA1 has the highest SOCME value of 7.45 $cm^{-1}$, while CMA4 has the lowest SOCME value of 0.97 $cm^{-1}$. The table reveals that activation energy is lower when there is small discrepancy between $\Delta E_{st}$ and $\lambda_{rISC}$ values, which leads to higher value of $K_{rISC}$.

In the CMA1 molecule, we observe a large change in torsion angle of about 88 degrees between the donor and acceptor ligands during transition from $S_0$ to $S_1$, while smaller changes in torsion angles of about 20 degrees have been observed in other molecules during this transition. Additionally, rotation between the donor and acceptor ligands also takes place during transition from $S_0$ geometry to $T_1$ geometry in all molecules. Due to these changes in molecular geometry at the excited states, we optimized each molecule at $S_1$ and $T_1$ geometry and taken their energy difference as the value of $\Delta E_{st}$, i.e., the adiabatic energy gap between $S_1$ and $T_1$. The large change in torsion angle observed as CMA1 transitions from $S_0$ geometry to $S_1$ geometry could play a part in the extremely high $K_{rISC}$ value of the order of $10^8$ $s^{-1}$ in gaseous phase. In 2017, Jelena et al. reported calculated $K_{rISC}$ value of the order of $10^8$ $s^{-1}$ for CMA1 in solvent [24] and in 2021, Lin et al. reported a $K_{rISC}$ value of $1.28 \times 10^{10}$ $s^{-1}$ for CMA1 in solid phase at 298.15K [30]. We anticipate higher $K_{rISC}$ value due to the close approach of $S_1$ and $T_1$ states caused by the rotation of carbazole ligands. The very low value of $K_{rISC}$ in CMA2 is due to the large discrepancy between $\Delta E_{st}$ and $\lambda_{rISC}$ leading to high activation energy.

## Conclusion

OLED technology has seen rapid development over the past few years and therefore has become more prevalent in consumer devices nowadays. As a result, scientists are looking for ways to increase their efficiency. Due to their potential of being able to achieve 100% fluorescence, TADF materials are becoming increasingly popular. However, the excited state kinematics requires more detailed and conceptual analysis prior to development of optoelectronic devices. Therefore, we investigated the electronic, optical and kinetic properties of five different gold-centered CMAs using DFT, and calculated the rate of reverse intersystem crossing

between the lowest excited singlet and triplet states. We find that the gold atom boosts the rate of rISC along with enhancing the spin-orbit coupling. Although our findings show that CMA1 has a remarkably high $K_{rISC}$ value of the order of $10^8$ $s^{-1}$, making it the perfect candidate to be a TADF emitter, its low PL intensity remains a concern. We observe that chemical modification of the carbazole ligands leads to an increase in PL intensities at the cost of reduced $K_{rISC}$ value. Therefore, an optimal trade-off between $K_{rISC}$ value and PL intensity must be achieved which introduces design challenges. In our study, we found CMA3 to be the most suitable candidate for light emission. Furthermore, we find that molecules with good donor-acceptor properties such as CMA1 and CMA2 show greater splitting of the first excited triplet state and also show a larger change in the torsion angle between donor and acceptor ligands during transition from $S_0$ to $T_1$ as compared to other molecules. The torsion angle changes significantly in CMA1 as it transitions from $S_0$ geometry to $S_1$ geometry, which have a relation with its high value of $K_{rISC}$ as rotational flexibility is often linked with effective rISC. CMA2 has the smallest value of $K_{rISC}$ as it has a large difference between $\Delta E_{st}$ and $\lambda_{rISC}$ values, rendering it unsuitable for TADF. Our work demonstrates that activation energy plays a very crucial role in rISC and we conclude that the rate of rISC depends on $\Delta E_{st}$, SOC and activation energy. We find that CMA1, CMA3 and CMA4 show promising properties for TADF. Experiments are required to obtain more accurate and useful information in these molecules, and enhance our understanding of the effect of SOC in rISC. For future work, computational investigation to obtain rISC rates between higher excited triplet states and first excited singlet state will be performed that is essential to understand excited state kinetics for molecules like CMA4 and CMA5 where the gap between $T_2$ and $S_1$ is very small.

**Data Availability**

Data will be made available on request.

**Acknowledgement**

The authors are grateful to one of our Organic Optoelectronic Simulation Group members Mr. Md. Asif for valuable discussion regarding spin-orbit coupling calculation with ORCA software.

**Conflict of Interest**

On behalf of all authors, the corresponding author states that there is no conflict of interest.

**References**

1. Tagare, J. and Vaidyanathan, S., 2018. Recent development of phenanthroimidazole-based fluorophores for blue organic light-emitting diodes (OLEDs): an overview. Journal of Materials Chemistry C, 6(38), pp.10138-10173.

2. Li, G., Xu, K., Zheng, J., Fang, X., Lou, W., Zhan, F., Deng, C., Yang, Y.F., Zhang, Q. and She, Y., 2024. High-performance ultraviolet organic light-emitting diodes enabled by double boron–oxygen-embedded benzo [m] tetraphene emitters. *Journal of the American Chemical Society*, *146*(2), pp.1667-1680.

3. Tang, C.W. and VanSlyke, S.A., 1987. Organic electroluminescent diodes. *Applied physics letters*, *51*(12), pp.913-915.

4. Adachi, C., Baldo, M.A., Thompson, M.E. and Forrest, S.R., 2001. Nearly 100% internal phosphorescence efficiency in an organic light-emitting device. *Journal of Applied Physics*, *90*(10), pp.5048-5051.

5. Hua, T., Cao, X., Miao, J., Yin, X., Chen, Z., Huang, Z. and Yang, C., 2024. Deep-blue organic light-emitting diodes for ultrahigh-definition displays. *Nature Photonics*, pp.1-9.

6.Chen, X.K., Kim, D. and Brédas, J.L., 2018. Thermally activated delayed fluorescence (TADF) path toward efficient electroluminescence in purely organic materials: molecular level insight. Accounts of Chemical Research, 51(9), pp.2215-2224.

7. Burroughes, J.H., Bradley, D.D., Brown, A.R., Marks, R.N., Mackay, K., Friend, R.H., Burns, P.L. and Holmes, A.B., 1990. Light-emitting diodes based on conjugated polymers. nature, 347(6293), pp.539-541.

8. Baldo, M.A., O'Brien, D.F., You, Y., Shoustikov, A., Sibley, S., Thompson, M.E. and Forrest, S.R., 2023. Highly efficient phosphorescent emission from organic electroluminescent devices. In Electrophosphorescent Materials and Devices (pp. 1-11). Jenny Stanford Publishing.

9. Chawdhury, N., Köhler, A., Friend, R. H., Wong, W. Y., Lewis, J., Younus, M., ... & Khan, M. S. (1999). Evolution of lowest singlet and triplet excited states with number of thienyl rings in platinum poly-ynes. *The Journal of chemical physics, 110(10), 4963-4970.*

10. Perrin, F. Fluorescence of solutions. Ann. Phys. (Paris, Fr.) 1929,10, 169−275.

11. Chen, T., Zheng, L., Yuan, J., An, Z., Chen, R., Tao, Y., Li, H., Xie, X. and Huang, W., 2015. Understanding the control of singlet-triplet splitting for organic exciton manipulating: a combined theoretical and experimental approach. Scientific reports, 5(1), p.10923.

12. Endo, A., Sato, K., Yoshimura, K., Kai, T., Kawada, A., Miyazaki, H. and Adachi, C., 2011. Efficient up-conversion of triplet excitons into a singlet state and its application for organic light emitting diodes. Applied Physics Letters, 98(8).
13. Uoyama, H., Goushi, K., Shizu, K., Nomura, H. and Adachi, C., 2012. Highly efficient organic light-emitting diodes from delayed fluorescence. Nature, 492(7428), pp.234-238.
14. Endo, A, Ogasawara, M, Takahashi, A, Yokoyama, D, Kato, Y & Adachi, C 2009, 'Thermally activated delayed fluorescence from Sn4+-porphyrin complexes and their application to organic light-emitting diodes -A novel mechanism for electroluminescence', Advanced Materials, vol. 21, no. 47, pp. 4802-4806.
15. Wang, L., Ou, Q., Peng, Q. and Shuai, Z., 2021. Theoretical characterizations of TADF materials: Roles of Δ G and the singlet–triplet excited states interconversion. *The Journal of Physical Chemistry A*, *125*(7), pp.1468-1475.
16. Cai, M., Auffray, M., Zhang, D., Zhang, Y., Nagata, R., Lin, Z., Tang, X., Chan, C.Y., Lee, Y.T., Huang, T. and Song, X., 2021. Enhancing spin-orbital coupling in deep-blue/blue TADF emitters by minimizing the distance from the heteroatoms in donors to acceptors. Chemical Engineering Journal, 420, p.127591.
17. Wang, Z., Jiang, X., Xiong, J., Xiao, B., Wang, Y., Zhou, X., Pan, R. and Tang, X., 2024. Understanding Spin–Orbit-Coupling-Induced Reverse Intersystem Crossing in DMAC-TRZ-Doped Organic Light-Emitting Diodes via Magnetic-Field-Effect Measurement. The Journal of Physical Chemistry Letters, 15, pp.9630-9636.
18. Kim, K.J., Kim, J., Lim, J.T., Heo, J., Park, B.J., Nam, H., Choi, H., Yoon, S.S., Kim, W., Kang, S. and Kim, T., 2024. Anthracene derivatives with strong spin–orbit coupling and efficient high-lying reverse intersystem crossing beyond the El-Sayed rule. Materials Horizons, 11(6), pp.1484-1494.
19. Justin Thomas, K.R., Lin, J.T., Tao, Y.T. and Ko, C.W., 2001. Light-emitting carbazole derivatives: potential electroluminescent materials. Journal of the American Chemical Society, 123(38), pp.9404-9411.
20. Jiang, H., Sun, J. and Zhang, J., 2012. A review on synthesis of carbazole-based chromophores as organic light-emitting materials. Current Organic Chemistry, 16(17), pp.2014-2025.
21. Romanov, A., Di, D., Yang, L., Conaghan, P., Jones, S., Friend, R., Linnolahti, M., Credgington, D. and Bochmann, M., 2018, September. Linear carbene metal amides as a new class of emitters for highly efficient solution-processed and vapor-deposited OLEDs (Conference Presentation). In Organic Light Emitting Materials and Devices XXII (Vol. 10736, p. 1073607). SPIE.
22. Phuoc, N.L., Brannan, A.C., Romanov, A.S. and Linnolahti, M., 2023. Tailoring Carbene–Metal–Amides for Thermally Activated Delayed Fluorescence: A Computationally Guided Study on the Effect of Cyclic (Alkyl)(amino) carbenes. Molecules, 28(11), p.4398.
23. Lv, X., Song, J., Fu, X., Guo, S., Gu, J., Meng, L. and Lu, C.Z., 2024. Enhancing Reverse Intersystem Crossing in Triptycene-TADF Emitters: Theoretical Insights into Reorganization Energy and Heavy Atom Effects. The Journal of Physical Chemistry A, 128(9), pp.1611-1619.
24. Föller, J. and Marian, C.M., 2017. Rotationally assisted spin-state inversion in carbene–metal–amides is an artifact. The Journal of physical chemistry letters, 8(22), pp.5643-5647.

25. Taffet, E.J., Olivier, Y., Lam, F., Beljonne, D. and Scholes, G.D., 2018. Carbene–metal–amide bond deformation, rather than ligand rotation, drives delayed fluorescence. The Journal of physical chemistry letters, 9(7), pp.1620-1626.
26. Li, P., Wang, Z., Wang, S., Zhou, C., Zhang, Y., Zheng, C. and Chen, R., 2021. Construction of High-Performance Carbene–Metal–Amide-Like TADF Materials: A Theoretical Study. The Journal of Physical Chemistry C, 125(48), pp.26770-26777.
27. Zobel, J.P., Wernbacher, A.M. and González, L., 2023. Efficient Reverse Intersystem Crossing in Carbene-Copper-Amide TADF Emitters via an Intermediate Triplet State. Angewandte Chemie International Edition, 62(15), p.e202217620.
28. Hamze, R., Peltier, J.L., Sylvinson, D., Jung, M., Cardenas, J., Haiges, R., Soleilhavoup, M., Jazzar, R., Djurovich, P.I., Bertrand, G. and Thompson, M.E., 2019. Eliminating nonradiative decay in Cu (I) emitters:> 99% quantum efficiency and microsecond lifetime. Science, 363(6427), pp.601-606.
29. Song, X.F., Li, Z.W., Chen, W.K., Gao, Y.J. and Cui, G., 2022. Thermally Activated Delayed Fluorescence Mechanism of a Bicyclic "Carbene–Metal–Amide" Copper Compound: DFT/MRCI Studies and Roles of Excited-State Structure Relaxation. Inorganic Chemistry, 61(20), pp.7673-7681.
30. Lin, S., Ou, Q., Wang, Y., Peng, Q. and Shuai, Z., 2021. Aggregation-enhanced thermally activated delayed fluorescence efficiency for two-coordinate carbene–metal–amide complexes: A QM/MM study. The Journal of Physical Chemistry Letters, 12(11), pp.2944-2953.
31. Shizu, K., Ren, Y. and Kaji, H., 2023. Promoting reverse intersystem crossing in thermally activated delayed fluorescence via the heavy-atom effect. The Journal of Physical Chemistry A, 127(2), pp.439-449.
32. Di, D., Romanov, A.S., Yang, L., Richter, J.M., Rivett, J.P., Jones, S., Thomas, T.H., Abdi Jalebi, M., Friend, R.H., Linnolahti, M. and Bochmann, M., 2017. High-performance light-emitting diodes based on carbene-metal-amides. Science, 356(6334), pp.159-163.
33. Kasha, M., 1950. Characterization of electronic transitions in complex molecules. Discussions of the Faraday society, 9, pp.14-19.
34. Redmond, R.W., Kochevar, I.E., Krieg, M., Smith, G. and McGimpsey, W.G., 1997. Excited state relaxation in cyanine dyes: a remarkably efficient reverse intersystem crossing from upper triplet levels. The Journal of Physical Chemistry A, 101(15), pp.2773-2777.
35. Xu, Q., Scully, A.D., Skidmore, M.A., Ke, H., Wu, X., Li, J., Zhang, Z., Li, X. and Ueno, K., 2024. Reverse intersystem crossing from high-level triplet excited electronic states of fluorescent organic molecules. Journal of Materials Chemistry C, 12(37), pp.15039-15050.
36. Pan, Y., Li, W., Zhang, S., Yao, L., Gu, C., Xu, H., Yang, B. and Ma, Y., 2014. High yields of singlet excitons in organic electroluminescence through two paths of cold and hot excitons. Advanced Optical Materials, 2(6), pp.510-515.
37. Wilson, J.S., Chawdhury, N., Al-Mandhary, M.R., Younus, M., Khan, M.S., Raithby, P.R., Köhler, A. and Friend, R.H., 2001. The energy gap law for triplet states in Pt-containing conjugated polymers and monomers. Journal of the American Chemical Society, 123(38), pp.9412-9417.
38. Gaussian 16W, M. J. Frisch et al., Gaussian, Inc., Wallingford CT, 2016.

39. Austin A, Petersson GA, Frisch MJ, Dobek FJ, Scalmani G, Throssell K. A Density Functional with Spherical Atom Dispersion Terms. J Chem Theory Comput. 2012 Dec 11;8(12):4989-5007. doi: 10.1021/ct300778e. Epub 2012 Nov 5. PMID: 26593191.
40. Neese, F., 2022. Software update: The ORCA program system—Version 5.0. Wiley Interdisciplinary Reviews: Computational Molecular Science, 12(5), p.e1606.
41. Forrest, S.R., 2020. Organic electronics: foundations to applications. Oxford University Press, USA.

**All Figure Captions**

**Fig. 1** A diagram illustrating thermally activated delayed fluorescence (TADF) mechanism. After holes and electrons are injected into the system, singlet and triplet excitons are formed in a singlet to triplet ratio of 1:3. The higher exciton states are transferred to the lowest exciton states ($S_1$ or $T_1$) via quick vibrational relaxation and internal conversion (IC). Then, through the rISC process, the triplet excitons at $T_1$ are transformed into singlet excitons at $S_1$ by means of thermal activation, instead of phosphorescence. The singlet excitons at $S_1$ radiatively drop to $S_0$ state, giving prompt fluorescence, and the newly formed singlet excitons via rISC process also drop to $S_0$, giving delayed fluorescence. Prompt fluorescence usually takes place in the order of nanoseconds, while delayed fluorescence can last up to microseconds. Therefore, fluorescence and delayed fluorescence have the potential to accumulate to about 100% fluorescence emission theoretically

**Fig. 2** Schematic potential surfaces of $S_1$ and $T_1$ showing the reorganization energy and activation energy

**Fig. 3** (a) Molecular structures and (b) optimized geometry of Carbene Metal Amides

**Fig. 4** HOMOs, LUMOs, their energies, and gaps between HOMOs and LUMOs ($\Delta E_{HL}$) of the simulated CMAs in their ground state geometry

**Fig. 5** Energy level diagram showing the lower lying five excited states at ground state geometry

**Fig. 6** $S_1$ and $T_1$ energy states of each molecule considering SOC and without considering SOC generated by ORCA5 using B3LYP functional

**Fig. 7** Optical absorption spectra and fluorescence emission spectra of all five CMA molecules

**Fig. 8** The HOMO and LUMO of each molecule at optimized $S_1$ and $T_1$ geometry

**Fig. 9** $K_{rISC}$ vs Activation energy graph for all the molecules showing a linear relationship

## Figures

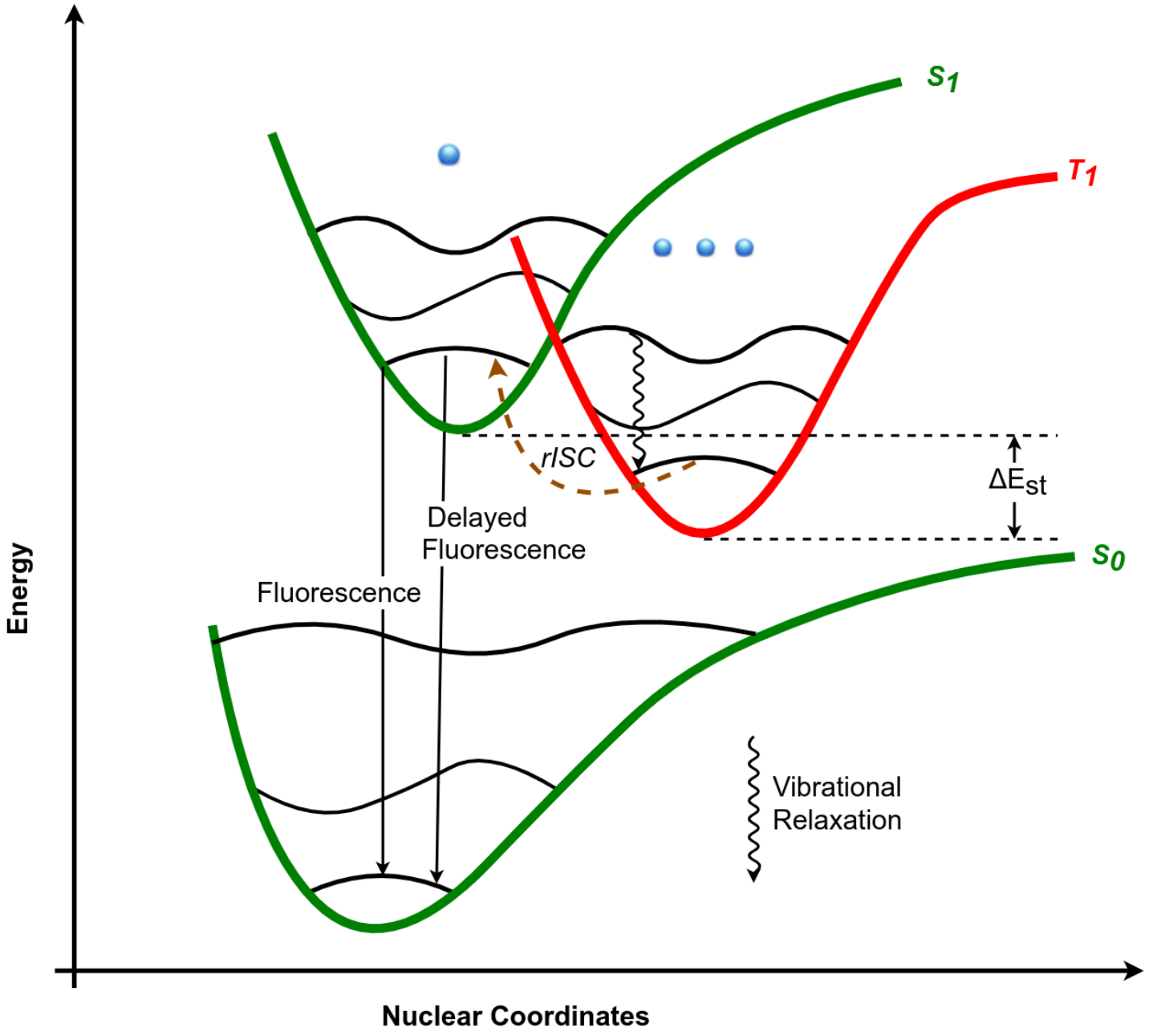



**Figure 1**

A diagram illustrating thermally activated delayed fluorescence (TADF) mechanism. After holes and electrons are injected into the system, singlet and triplet excitons are formed in a singlet to triplet ratio of 1:3. The higher exciton states are transferred to the lowest exciton states ($S_1$ or $T_1$) via quick vibrational relaxation and internal conversion (IC). Then, through the rISC process, the triplet excitons at $T_1$ are transformed into singlet excitons at $S_1$ by means of thermal activation, instead of phosphorescence. The singlet excitons at $S_1$ radiatively drop to $S_0$ state, giving prompt fluorescence, and the newly formed singlet excitons via rISC process also drop to $S_0$, giving delayed fluorescence. Prompt fluorescence usually takes place in the order of nanoseconds, while delayed fluorescence can last up to

microseconds. Therefore, fluorescence and delayed fluorescence have the potential to accumulate to about 100% fluorescence emission theoretically

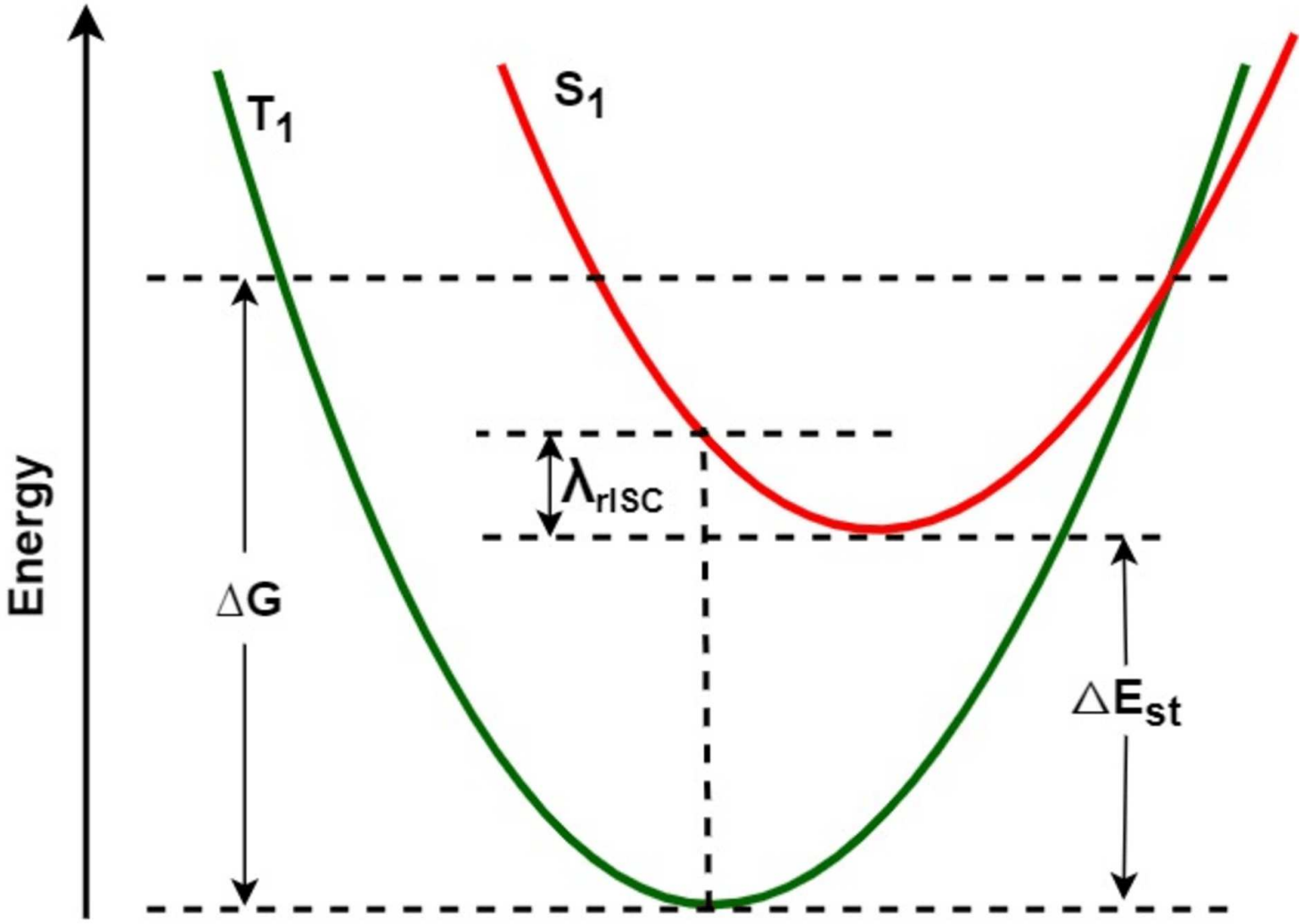



**Figure 2**

Schematic potential surfaces of $S_1$ and $T_1$ showing the reorganization energy and activation energy

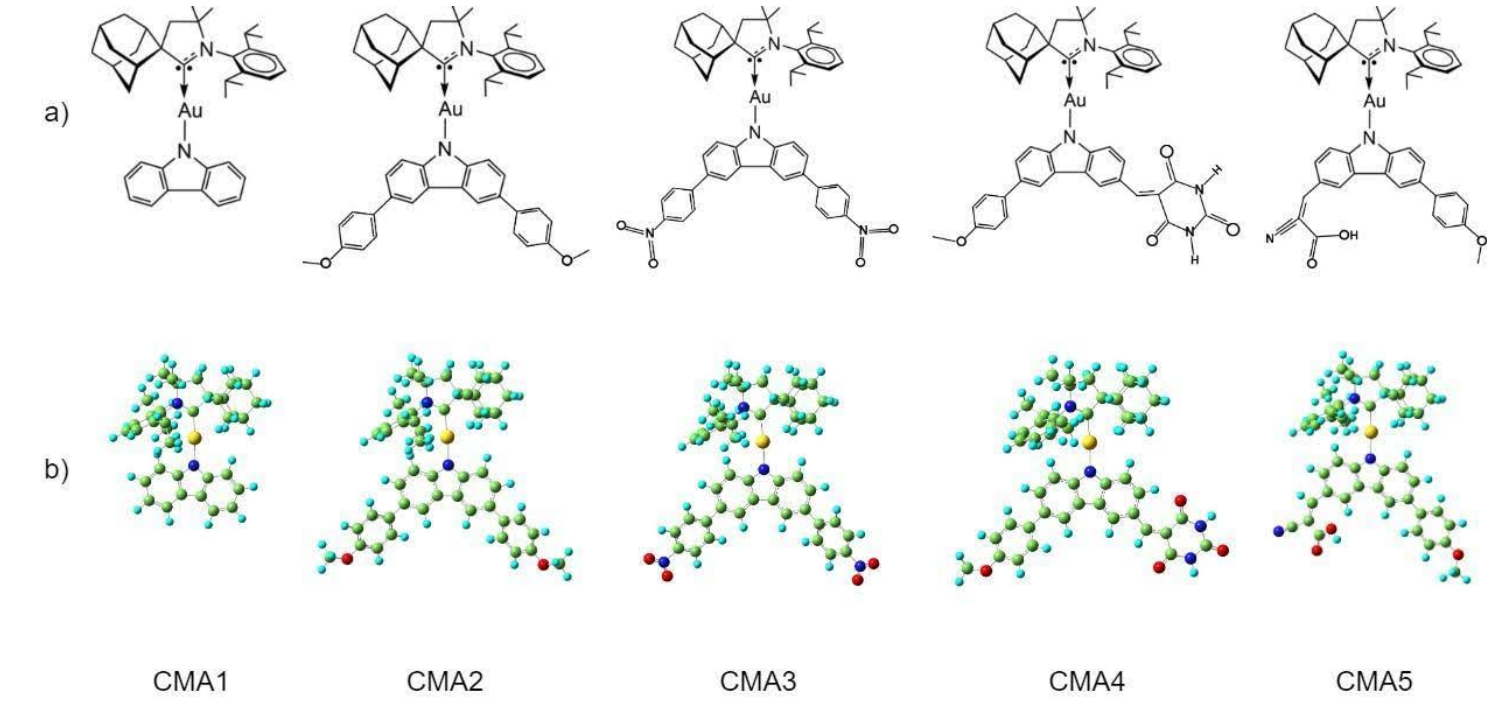



**Figure 3**

(a) Molecular structures and (b) optimized geometry of Carbene Metal Amides

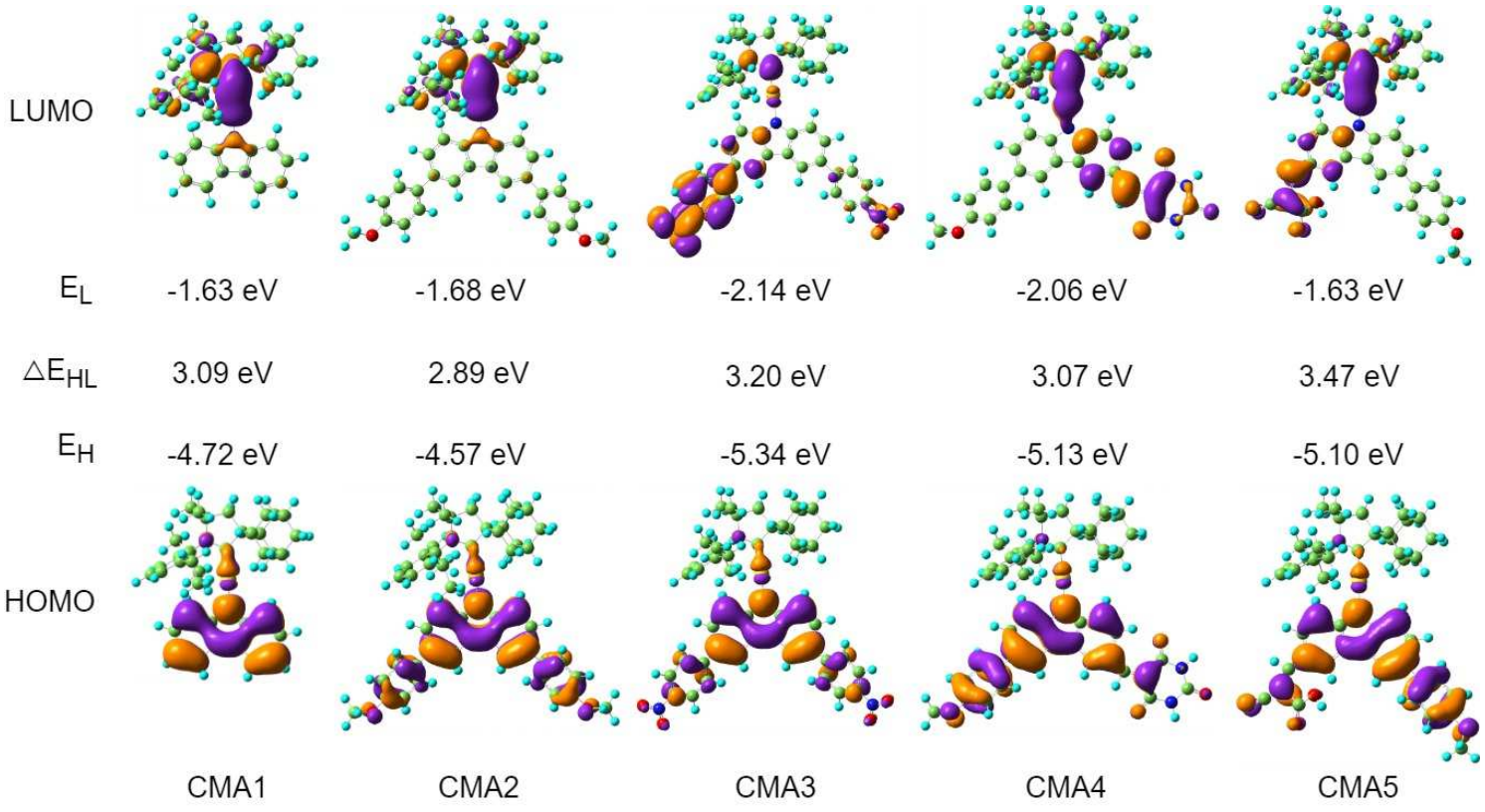



**Figure 4**

HOMOs, LUMOs, their energies, and gaps between HOMOs and LUMOs ($\triangle E_{HL}$) of the simulated CMAs in their ground state geometry

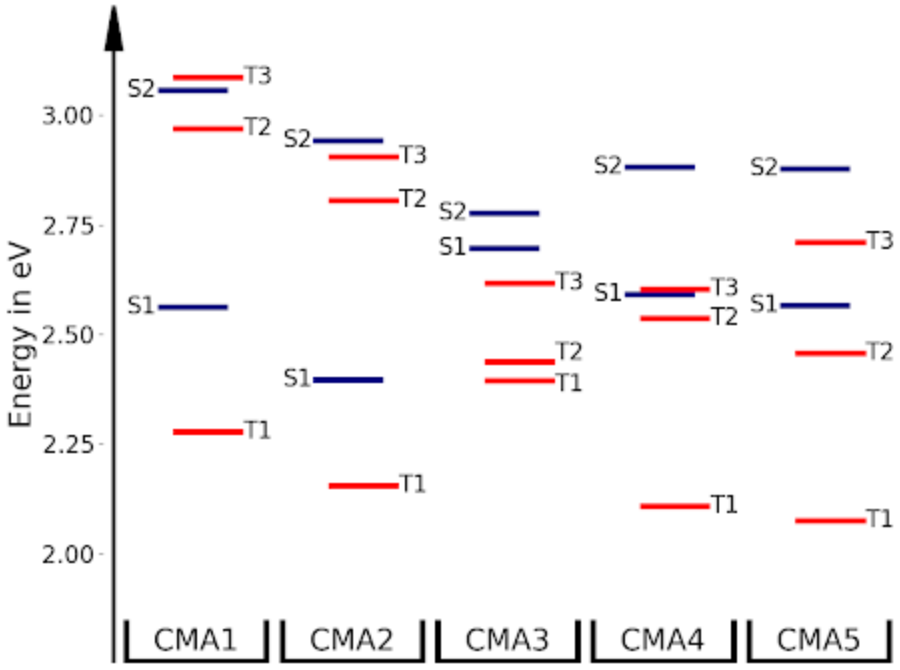



**Figure 5**

Energy level diagram showing the lower lying five excited states at ground state geometry

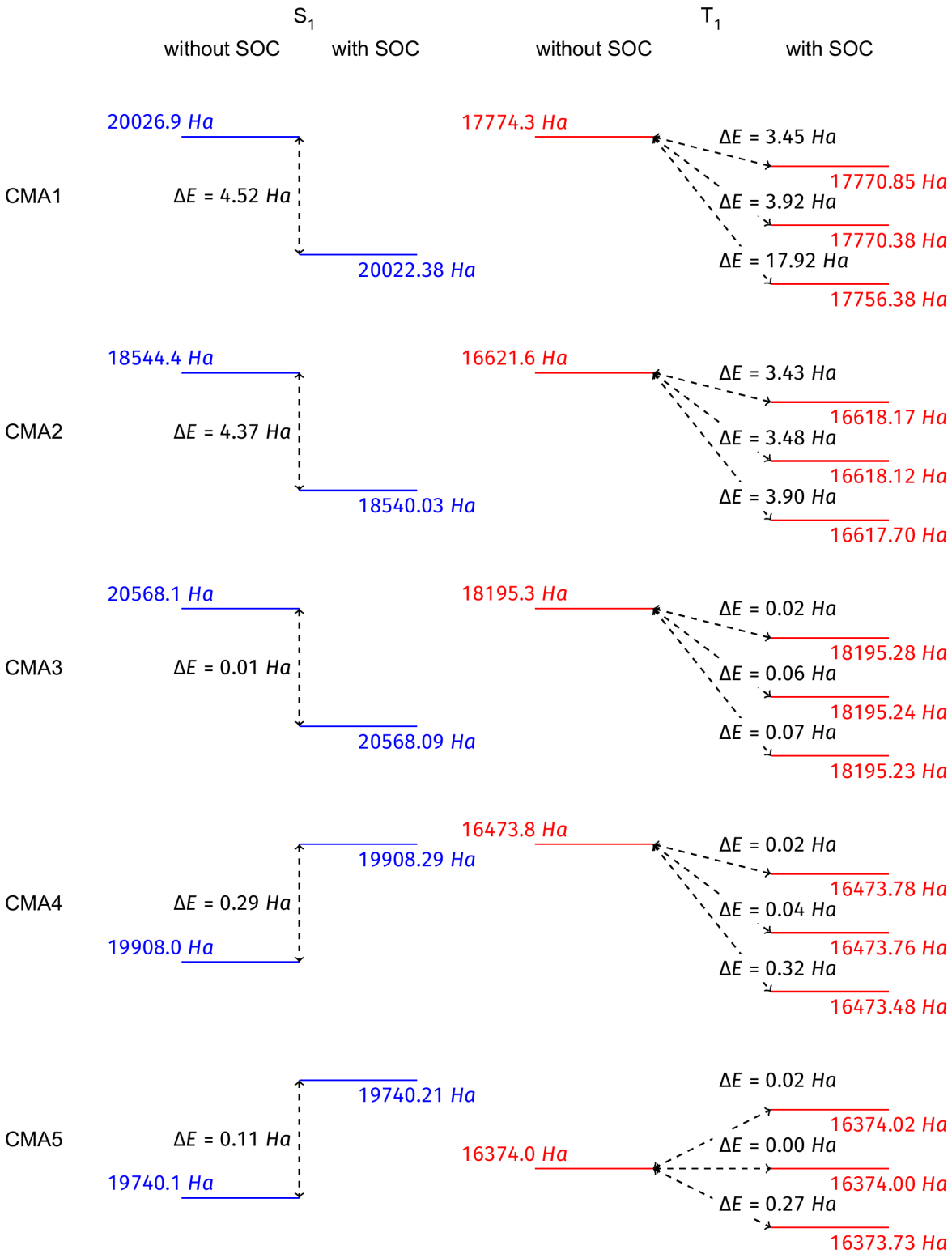



**Figure 6**

$S_1$ and $T_1$ energy states of each molecule considering SOC and without considering SOC generated by ORCA5 using B3LYP functional

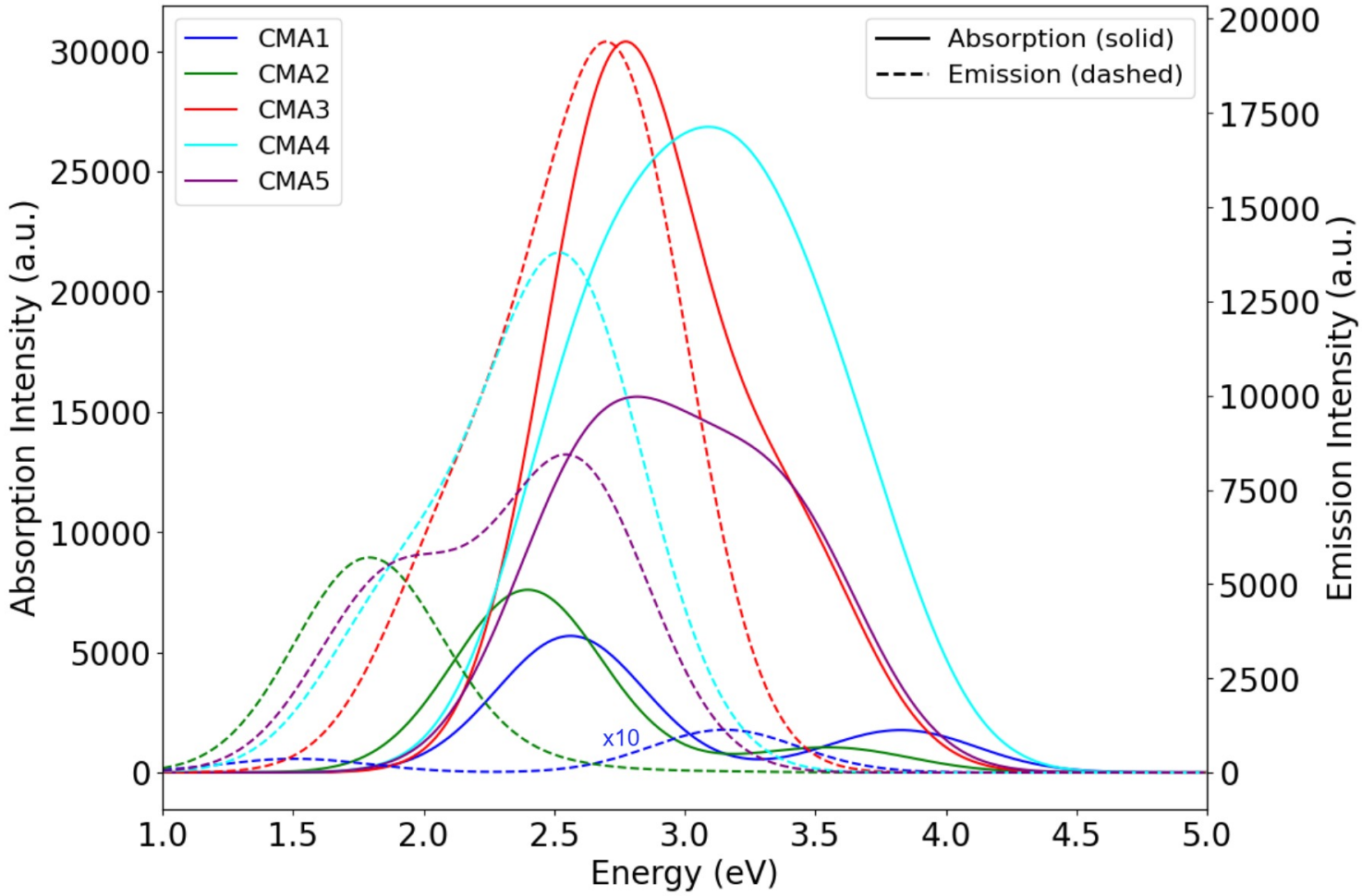
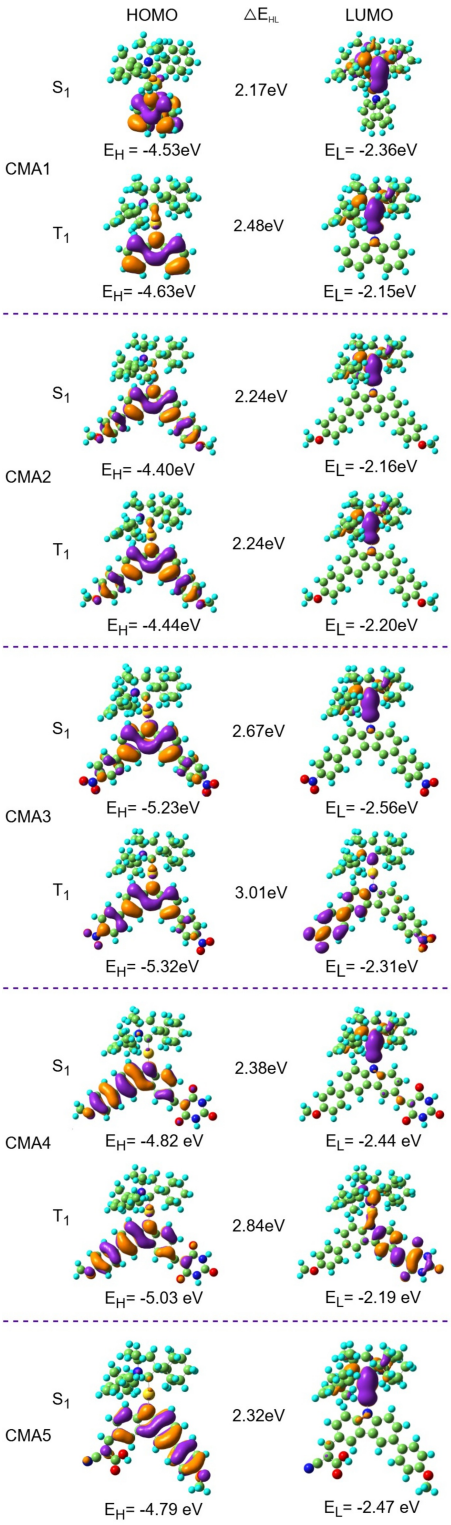



**Figure 7**

Optical absorption spectra and fluorescence emission spectra of all five CMA molecules




## Figure 8

The HOMO and LUMO of each molecule at optimized $S_1$ and $T_1$ geometry

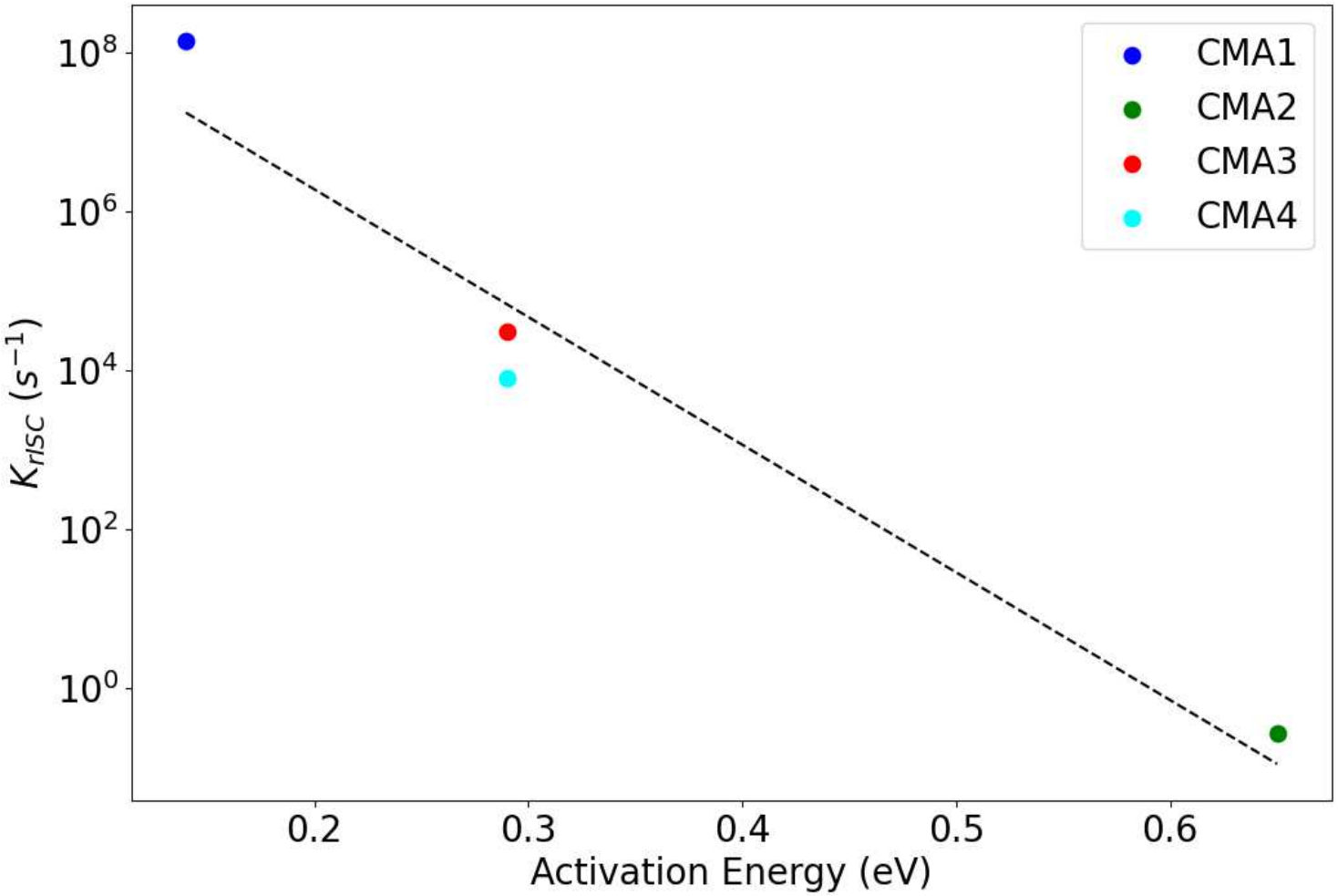



**Figure 9**

$K_{rISC}$ vs Activation energy graph for all the molecules showing a linear relationship

## Supplementary Files

This is a list of supplementary files associated with this preprint. Click to download.

- Table1.docx